In-Plane Displacement Detection With Picometer Accuracy on a Conventional Microscope

Jaap Kokorian, Federico Buja, and Willem Merlijn van Spengen

***Abstract*— In this paper, we present a new method for detecting in-plane displacements in microelectromechanical systems (MEMS) with an unprecedented sub-ångström accuracy. We use a curve-fitting method that is commonly employed in spectroscopy to find peak positions in a spectrum. We fit a function to the intensity profile of the image of a silicon beam that was captured with a CCD camera on an optical microscope. The position resolution depends on the amount of pixel noise and on how the moving feature is spread across the detector pixels. The resolution is usually limited by photon shot noise, which can be controlled and lowered in several ways. To demonstrate the technique we measure the adhesion snap-off of two silicon surfaces. We assess the accuracy of the technique using two different silicon MEMS devices and an experimental ultrananocrystalline diamond device. The lowest position noise that we report is obtained by summing 1577 image lines and is as low as 60 pm root mean square. [2014-0040]**

***Index Terms*— Displacement measurement, optical noise, optical image processing, optical position measurement, MEMS, subpixel resolution.**

I. Introduction

A. The Observation of Motion in MEMS

SINCE THE advent of microelectromechanical Systems (MEMS) in the 1980's, many measurement techniques have been used to study the lateral and out-of-plane motions of these tiny devices. Although capacitive sensing is commonly used in commercial products like accelerometers and gyroscopes, this method has disadvantages when used in the lab due to the fact that parasitic capacitances cause excessive noise if the readout chip is not monolithically integrated with the moving MEMS [1], or at least placed right next to it in the same package. Also, it is difficult to unambiguously detect motion if it occurs in more then one dimension at the same time, and detection speed is often limited.

For this reason, many optical motion detection methods are in use as well. Commonly applied for out of plane motion assessment is laser Doppler vibrometry [2], TV holography [3] or interferometry, either with continuous illumination [4] or stroboscopic illumination [5]. All these techniques have in common that they provide a considerably higher precision than the optical resolution limit, caused by the wavelength of the light with which the object is being imaged. They accomplish this, in one way or another, by making use of the wave nature of light.

It is difficult to use interference to enhance in-plane motion detection, which is why considerably fewer techniques are available, and they are not employed as often as the out-of plane methods [6]. However, in-plane motion detection is important because many MEMS devices exhibit in-plane motion of some sort, comb drive actuators being a notorious example. Typical motion ranges are in the microns but can usually be controlled down to the nanometer level. The high accuracy of these actuators calls for detection methods to be considerably better than the raw resolution that can be obtained by simple optical imaging. The resolution of optical microscopy is limited roughly by the wavelength of the light being used, which is known as the Rayleigh criterion or the optical diffraction limit. In a typical high-quality microscope this amounts to around 500 nm. In this paper, we present a powerful method to circumvent this limit.

B. In-Plane Motion Detection Techniques Circumventing the Resolution Limit

Several methods exist that enhance the resolution of in-plane motion detection beyond the Rayleigh criterion to monitor the motion of MEMS devices.

For studies on relatively large-scale motion, as in the assessment of the reliability of the rotating gear train MEMS devices of Sandia National Laboratories [7], no sub-wavelength resolution was actually required. Simple edge enhancement was sufficient to obtain an accurate measure for the rotational angle of the cogwheels. To follow the fast moving microscopic parts, stroboscopic illumination was employed.

Widely used is digital image correlation [8], [9], a method that has been investigated thoroughly by Davis & Freeman [10]. Guo *et al.* [11] use a similar technique based on optical flow: a mathematical concept that formalizes the concept difference between two images in terms of motion, which can be calculated using image correlation.

The basic principle is that a shifted version of an image of a device at rest, the 'template', is used to find the position of the device in another image that is made when displacement has taken place. The image of the device is assumed to be constant in shape and intensity, and hence by shifting the

Manuscript received February 10, 2014; revised May 30, 2014; accepted June 25, 2014. Date of publication July 17, 2014; date of current version June 1, 2015. This work was supported by the Dutch Netherlands Organisation for Scientific Research-Stichting voor Technologie en Wetenschap Foundation, Utrecht, The Netherlands, through the Vidi Program under Grant 10771. Subject Editor C. Rembe.

J. Kokorian and F. Buja are with the Precision and Micro Engineering Group, Delft University of Technology, Delft CD 2628, The Netherlands (e-mail: j.kokorian@tudelft.nl; f.buja@tudelft.nl).

W. M. van Spengen is with the Precision and Micro Engineering Group, Delft University of Technology, Delft CD 2628, The Netherlands; and also with Falco Systems B.V., Amsterdam 1083 BA, The Netherlands (e-mail: w.m.vanspengen@tudelft.nl).

Color versions of one or more of the figures in this paper are available online at http://ieeexplore.ieee.org.

Digital Object Identifier 10.1109/JMEMS.2014.2335153

template image progressively with respect to the new image B and calculating the correlation for every position, a maximum can be found in the correlation function that corresponds to the new position. To find this position accurately, the template image needs to be displaced by sub-pixel amounts, which means that a new image needs to be generated by interpolation between the pixels of the original template. Results with nanometer resolution can be obtained, and even sub-nanometer if spatio-temporal filtering is employed [12], [13]. The latter technique however, requires the motion of the device to be smooth, without any jerks or sudden stops. If the motion is jerky, this will be smoothed due to the filtering.

Powerful as the technique may be, one drawback seriously limits the accuracy with which motion can be detected. Kleinemeier [14] and Davis *et al.* [15] have shown that the interpolation required to obtain the shifted version of the template image causes systematic errors when noise is present in the system. These errors are more or less sinusoidally varying over the displacement by less than a single pixel. Under extreme circumstances, this can result in systematic position determination errors up to a significant portion of a single image pixel. Although the use of proper light conditions and sophisticated detection algorithms can mitigate the effect to a large extent, the error is always there at some level.

A technique reported by Yamahata *et al.* [16] uses Fourier analysis with great success. They extract the position of a feature from the phase of the discrete spatial Fourier transform of an image. When analyzing a time-series of images, typically a movie of a moving device, the movement of the feature can be tracked by observing how the phase-shift of the principal peak in the frequency spectrum changes. The technique works especially well with periodic features, multiple parallel beams for example. The resolution depends strongly on the number of feature periods and can become as precise as 0.2 nm (root-mean-square).

Burns *et al.* [17] use a clever approach for high speed imaging. They designed a setup in which they could follow fast resonances of MEMS devices by investigating how much motion-related blur would appear when an image was taken with a long acquisition period compared to the period of the motion, which they called the 'blur-synthesis technique'. The amount of motion-induced blur was investigated by adjusting a reference image of the same device at rest by calculating what it would look like if a certain amount of motion-induced blurring would take place. By comparing these artificial images with the measured images containing motion-induced blur using χ^2-minimization, they were able to extract very precise resonance curves using a relatively standard microscopy system.

A technique that recently reported, with which very high resolution can be reached (<1.8 nm), is based on a MEMS-based movable grating that rotates due to the motion of linearly moving comb drives [18] of which the motion is to be determined. The direction of the reflection of a laser which is incident on the grating changes with the rotation, which allows a type of detection that is quite similar to the detection of out-of-plane cantilever motion in atomic force microscope (AFM) systems. The laser light is incident on a photosensitive detector and changes in illumination can be very accurately monitored. Disadvantage of this technique is of course that it requires dedicated structures, and hence it cannot be used on most devices. Also, the detection is only indirect: the rotation of a dedicated structure is monitored instead of the primary linear motion.

We may conclude that there are many techniques available that provide a better in-plane displacement resolution than the optical diffraction limit. However, many of these techniques are limited by periodic errors, cannot be used for measurements of 'jerky' motions, or require the integration of complicated mechanical structures. Yamahata *et al.* [16] reports the lowest position noise so far using Fourier analysis. Can we do better?

The technique that we report on in the current paper is based on fitting a mathematical model of the intensity variations of the image to detect motion between images. Pioneered for imaging by Hachicha and Simon [19], this is a very powerful technique that, to our knowledge, has never been applied to MEMS device monitoring. It is similar to the way the position of a peak is found in a spectrogram, for example to detect shifts in the Raman spectrum of mono-crystalline silicon under the influence of mechanical stress [20].

II. Method and Theory

We will explain our technique using the comb drive based nano battering ram [21] shown in figure 1a. For our purposes here, the intended function of the device (measuring adhesion) is not important. We could have used any linear MEMS actuator.

The inset of figure 1a shows a close-up of the ram, the counter-surface and the anchor point for one of the springs. An even smaller area with just two sections of the support springs is shown in to the right. The left beam is a small section of the support spring close to the ram and the right beam is a section of the support spring close to the anchor. When the ram moves, the left beam will move with it, but the right beam remains stationary.

The pixel intensities of each image line plotted against the pixel x-position will show a similar 'intensity profile' with two distinct peaks of which the positions corresponds to the positions of the two beams. When the intensity profiles of all lines are summed, a much smoother curve is obtained, as is shown in Figure 1b. If we manage to find a mathematical function that roughly matches the shape of a peak, we can apply a curve-fitting algorithm to find the value of the parameter that describes its center position. This technique is routinely used in many kinds of spectroscopy. A thorough investigation into the uncertainty of extracted peak position has recently been conducted by W. M. van Spengen [22] and we will use his theory here to investigate which parameters influence the measurement precision.

There are several ways to choose an appropriate fit-function to match the shape of the intensity profile. One way is to mathematically 'design' an algebraic function that resembles the intensity profile. The function should have a parameter x_0 that determines its horizontal shift. The advantage of this

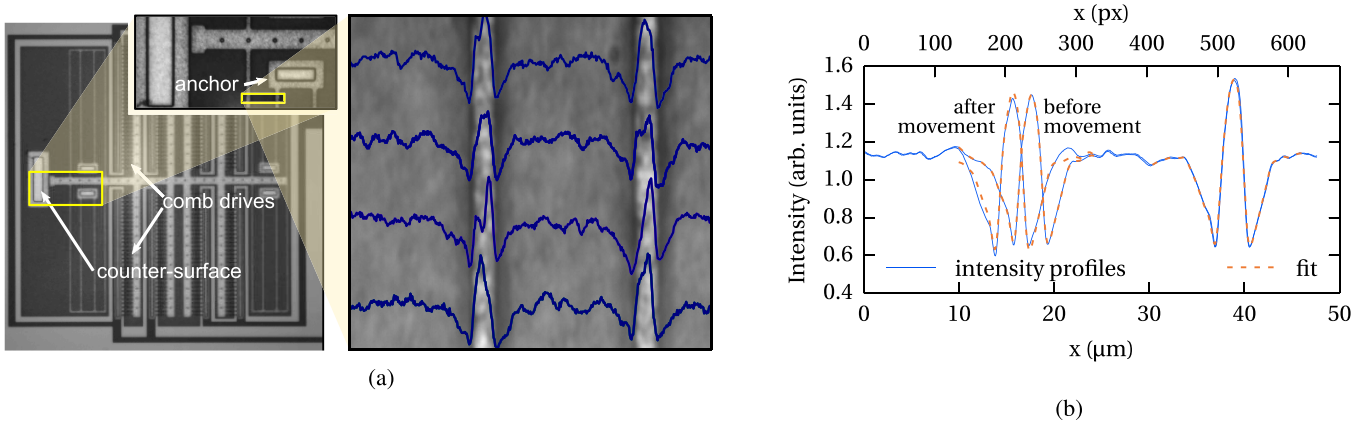

(a) (b)

Fig. 1. Illustration of the curve fitting procedure for detecting sub-pixel displacements. Figure 1a shows a 'nano ram' MEMS adhesion sensor [21]. The ram can be moved by a comb drive actuator until it makes contact with a counter-surface. To measure displacement of the ram, a small region of interest is selected that shows two beams of which one remains stationary and one shows the same movement as the ram. Each horizontal line of pixels shows a similar intensity profile of which four are plotted as an overlay. Figure 1b shows the intensity profile that results from vertically summing over all the pixels of the region of interest before and after the left beam has been displaced by about 27 pixels. By fitting a function with a center position parameter, $f(x, x_0)$ to both the left and right peak separately, the position 'x_d' of the left beam with respect to the right beam is found using $d = x_{0,\text{left}} - x_{0,\text{right}}$.

method is that it is impossible to accidentally incorporate some of the noise in the fit function. The disadvantage is that a specific function is required for every different type of intensity profile.

A more practical approach is to extract the function from the intensity profile itself by creating an algebraic representation of it in the form of a spline interpolation function $s\,(x)$. Splines can be created automatically from any array of data by most data-analysis programs. This technique has the disadvantage that all the noise on the profile is also incorporated in the spline function which introduces periodic errors [15]. It should therefore be smoothed or filtered to get rid of the noise. The spline can then be used as a fit function by modifying it with a shift-parameter 'x_0' and optionally a variable amplitude 'A' and offset 'y_0' as shown in equation (1).

$$f(x) = A \cdot s(x - x_0) + y_0 \tag{1}$$

Parameters A and y_0 are not essential, but can help the fit algorithm converge more easily if the amplitude of the intensity profile varies somewhat due to light source intensity fluctuations because of focal drift during a long measurement.

A. Uncertainty Analysis

The uncertainty of the fitted parameter x_0 is determined by the amount of noise on the intensity profile and the number of pixels that the 'moving part' of the intensity profile is spread across [20], [22].

The camera pixel noise has four components: electronic read noise, quantization noise, dark current, and photon shot noise. Read noise originates in the electronic read-out circuitry of the image sensor. Dark current refers to the current of electrons that are spontaneously freed, without a photon actually hitting the sensor. The amount of dark-current electrons per second depends exponentially on the sensor temperature. In applications that involve very long exposure times or little light, such as Raman spectroscopy and astronomy, the dark current typically dominates the noise figure, which is why CCD sensors used in Raman spectroscopes and large telescopes are often cooled with liquid nitrogen. In bright field microscopy the read noise and dark current are usually orders of magnitude lower than quantization noise and shot noise so we will further disregard them in this paper for the sake of brevity.

1) Shot Noise: Photon shot noise is caused by the fact that for a constant light intensity, the number of photons that are detected within a certain exposure time will vary. This is a fundamental property of light itself and has nothing to do with the architecture of the camera or the light source. Shot noise can be described as a Poisson process with parameter $\lambda = N_{\text{photons,px}}$. The signal to shot-noise ratio is given in equation (2),

$$\text{SNR}_{\text{shot}} = \frac{N_{\text{photons,px}}}{\sqrt{N_{\text{photons,px}}}} = \sqrt{N_{\text{photons,px}}} \tag{2}$$

where '$N_{\text{photons,px}}$' is the number of detected photons. The only way to increase it, is to maximize the amount of light that is captured by the sensor. The lower limit of shot noise is then determined by the number of photons that a pixel can detect before it saturates: the full-well-depth (FWD). The full-well-depth is usually expressed as the maximum number of electrons that can be stored on a pixel capacitor.

Important to remember is that the shot noise is related directly and exclusively to the pixel intensity, but in a slightly counter intuitive way: more photons means more shot noise. However, because the noise is equal to the square-root of the amount of photons, the net effect is positive and the signal-to-noise ratio increases for a higher number of photons. Equivalently, the relative uncertainty of a pixel value due to shot noise decreases.

2) Quantization Noise: Quantization noise originates from the limited amount of digitization levels available for digitizing a pixel intensity. Most CMOS and CCD cameras have an analog-to-digital converter (ADC) with a bit-depth of 8, 12 or 16 bits, yielding 256, 4096 or 65 536 quantization levels. Quantization noise is a random process with an approximately

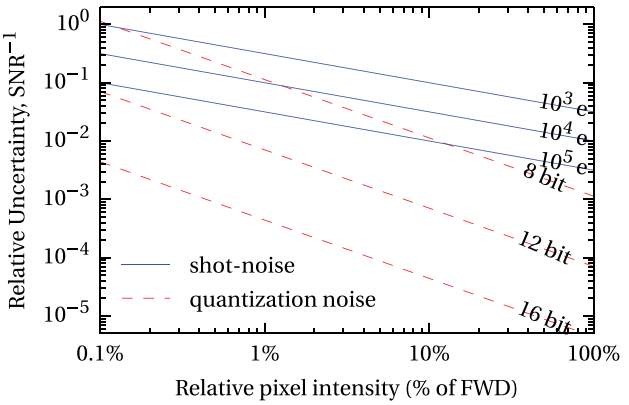

Fig. 2. The noise-to-signal ratio per pixel due to shot noise and quantization noise versus the relative pixel intensity $\frac{I_{px}}{I_{FWD}}$. The quantization noise is shown for sensors with 8, 12 and 16 bits AD-converters. The shot-noise is drawn for sensors with a full-well depth of 1000, 10 000 and 100 000 electrons.

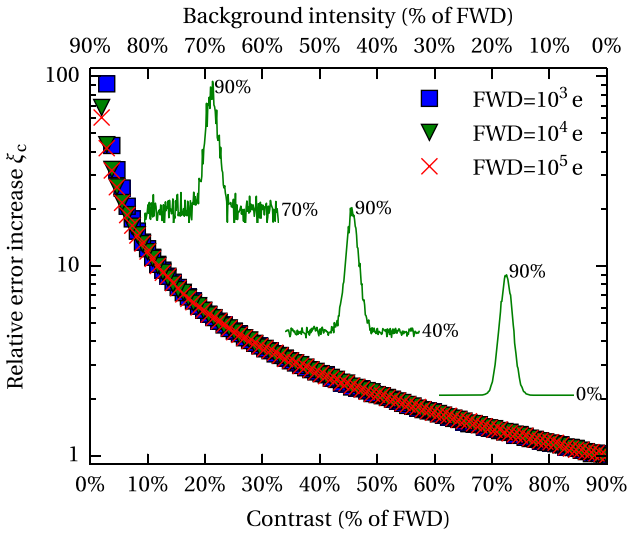

Fig. 3. The relative increase in the position error that results from the curve fitting algorithm due to limited contrast. Generated using a Monte Carlo simulation with $N_{MC} = 10000$. The maximum value of the peak was kept at 90 $\%_{FWD}$ while the background intensity was varied.

uniform probability density function. The signal to quantization noise ratio 'SNR_q' is given in equation (3).

$$SNR_q = \frac{I_{px}}{I_{FWD}} \frac{1}{\sqrt{12} \cdot \left(2^{N_{bits}} - 1\right)} \tag{3}$$

Where I_{px} is the pixel intensity, I_{FWD} is the full-well-depth and N_{bits} is the number of digitization bits.

3) Total Pixel Noise: The relative contributions of shot noise and quantization noise are shown in figure 2. The pixel intensity is expressed as a percentage of the full-well-depth, which is a fixed number for a given camera that may vary a little per pixel. It can only be increased by buying a different camera or by adding the analog values of a number of adjacent pixels before they are digitized by the camera ADC. Figure 2 shows that for cameras with a full-well-depth around a thousand electrons, the error is always determined by the shot noise. The bit-depth of the ADC can become an issue when pixel values are 'binned' before quantization. Binning an amount of N_{px} pixels effectively increases the full-well-depth by a factor N_{px} and consequently increases the signal-to-shot noise ratio by a factor $\sqrt{N_{px}}$, making the quantization noise the dominant source of noise.

4) Image Contrast: Thus far we have dealt with the noise of a single pixel, but to understand the contribution of image contrast to the eventual position detection noise we need to consider the intensity profile as a whole. Because we are fitting a parameter that corresponds to horizontal shift, the curve fit accuracy is not influenced by the addition of a constant offset to the intensity profile. This means that the presence of a non-zero background does not add anything to the position noise directly. However, because the maximum value that any pixel can have is physically limited to the full-well-depth of the image sensor, having a non-zero background effectively reduces the amount of pixel values available for the peak and reduces the signal-to-noise ratio.

In addition, any non-zero pixel automatically contains shot noise (see equation (2)), so the brighter the background, the more noise it contains. Because having a lighter background automatically means having less contrast (because of the upper limit of determined by the FWD), the peak will drown in the shot noise of the background pixels. The dominant source of noise is now still shot noise, but it originates from the background, not from the signal.

We have modeled the effect of having a brighter background and smaller contrast by doing a Monte Carlo simulation of a simple Gaussian peak with an offset and simulated shot noise. The maximum peak value was kept at 90 $\%_{FWD}$ while the background intensity was varied from 0 $\%_{FWD}$ to 90 $\%_{FWD}$ for three different values of the full-well-depth. For each combination of parameters we simulated 1000 realizations of the Gaussian intensity profile and performed a curve fit to obtain an estimate for the center of the peak.

Figure 3 shows the standard deviation of the peak position parameters of the 10 000 realizations of the Gaussian intensity profile. The values are normalized to the lowest value, which is obtained for a background intensity of 0 $\%_{FWD}$ and a corresponding contrast of 90 $\%_{FWD}$. When the background intensity approaches 90 $\%_{FWD}$, the contrast goes to 0 $\%_{FWD}$ and the fit error goes to infinity. The graph clearly shows that the relative error increase due to the presence of a non-zero background is independent of the absolute value of the full-well-depth.

In a real measurement the contrast will be determined mainly by the material and surface texture of the sample that is being imaged, and of the quality and focus of the optics that are used. If the peak is out of focus or if the optics are not diffraction limited, a smaller contrast will result.

5) Resolution and Pixel Binning: The uncertainty of the position parameter x_0 that is found with the curve fit procedure also depends on the resolution of the camera. Or more precisely, on the amount of pixels the 'beam'-part of the intensity profile is spread across.

Binning a number of N_{px} adjacent pixels has the combined effect of lowering the effective resolution and raising the

effective intensity per pixel which increases the signal-to-shot noise ratio $\mathrm{SNR}_{\mathrm{shot}}$. W. M. van Spengen [20], [22] has demonstrated that the negative effect of the decreased resolution is exactly compensated by the positive effect of the increase of the signal-to-shot noise ratio.

However, this theory is only true when we consider only a single line of pixels and we are binning the pixels horizontally. When binning pixels vertically, the resolution remains the same, but the signal intensity increases with the number of vertically binned pixels N_{lines} which increases the signal-to-shot noise ratio by a factor $\sqrt{N_{\mathrm{lines}}}$. Vertical binning can sometimes be performed on the sensor chip itself, but it amounts to exactly the same thing as vertically summing over a number of lines after the image has been captured.

6) Optical Magnification: The knowledge that spreading the signal over a larger number of pixels does not affect the position uncertainty [22] has an interesting consequence for the amount of optical magnification required. Placing a magnifying lens in front of the camera or increasing the camera resolution (by choosing a different camera) will spread the signal over a larger number of pixels, but the total amount of light that is captured will remain the same. This lowers the average pixel intensity and consequently decreases the signal-to-shot noise ratio $\mathrm{SNR}_{\mathrm{shot}}$, which according to the theory is counteracted exactly by the positive effect of spreading the signal over a larger number of pixels. When acquisition speed is not an issue, the exposure time of the camera can be increased to increase the pixel intensity. This allows more light to reach the sensor and lowers the position uncertainty.

If the sample is illuminated through the microscope objective, an objective with a higher magnification will cause more light to be focused on the area of interest, which increases the signal-to-shot noise ratio $\mathrm{SNR}_{\mathrm{shot}}$ and directly results in a lower position uncertainty. Again, this happens because more photons are captured from the interesting part of the intensity profile, not because it is spread across a larger number of pixels.

7) Periodic Structures: When the maximum amount of light possible for the optical assembly has been reached, the only way to further decrease the uncertainty of the fitted parameter is to spread the signal over more pixels by making the feature that is fitted wider, for example by looking at a periodic pattern of beams instead of just a single beam. This effectively increases the signal-to-shot noise ratio, in this case by increasing the amount of information in the signal. Fitting a single function through a pattern of beams will result in a shot noise reduction of $\sqrt{\frac{1}{N_{\mathrm{periods}}}}$, where N_{periods} is the number of beams, resulting in a proportionally lower position noise. This is exactly the same as fitting a function through each beam in the pattern, determining the position of each individual beam and averaging the results. Because the noise is statistically independent for each pixel, the uncertainty decreases with the square-root of the number of averaged values (standard error). This trend corresponds to the recommendation by C. Yamahata *et al.* [16] to use a large number of periodic structures to get a higher precision, when using the Fourier transform method mentioned earlier. The highest resolution found by S. Petitgrand [13] was obtained on a high contrast sample with a highly textured surface. Translated to our technique, this would be equivalent to observing the collective motion of hundreds of narrow peaks simultaneously.

8) Total Position Error: We can summarize the findings of this section with a rule-of-thumb: make sure that the noise per pixel is dominated by shot-noise. When that is the case, the position detection error σ_{pos} is given by equation (4).

$$\sigma_{\mathrm{pos}} \sim \frac{1}{\sqrt{N_{\mathrm{photons,px}}}} \cdot \frac{1}{\sqrt{N_{\mathrm{lines}}}} \cdot \frac{1}{\sqrt{N_{\mathrm{periods}}}} \cdot \xi\,(\mathrm{c}) \qquad (4)$$

Where '$N_{\mathrm{photons,px}}$' is the average number of signal photons per pixel (i.e. the pixel intensity), 'N_{lines}' is the number of lines that are averaged or the vertical pixel binning amount, 'N_{periods}' is the number of periods of the pattern that is being imaged and $\xi\,(\mathrm{c})$ is the effective error increase due to limited contrast (see figure 3).

III. Experiments

To demonstrate the merits of the curve-fitting technique, we will show several measurements using three different MEMS actuators: the nano-ram adhesion sensor comb drive [21] shown in figure 1a that we used earlier in this paper to explain the technique, a 'Leiden MEMS tribometer' [23] and a novel nitrogen-incorporated ultrananocrystalline diamond (N-UNCD) based adhesion sensor [24]. The intensity profiles of their beam springs look slightly different, but the devices are similar in design.

The devices are placed under a Motic PSM-1000 optical microscope with a Motic ULWD50x objective and an additional $2\times$ magnifier lens, giving a total magnification of $100\times$. The sample is illuminated through the microscope objective with a Motic MLC150C halogen cold light source at its maximum intensity ($>120\,000$ lx). The images are taken with an Apogee Alta F4000 interline-scan CCD camera with an average pixel full-well depth of 31 000 electrons and a 16-bit analog-to-digital converter. This ensures the quantization noise can be neglected under all circumstances (see figure 2).

For all measurements the microscope is focused on a small area that shows a pair of support springs of which one moves with the translating part of the actuator and one remains stationary with respect to the substrate. To eliminate any unintended motion of the camera with respect to the sample we will only consider the motion of the actuated beam with respect to the stationary beam. The displacement of the actuated beam is calculated by creating separate splines for the moving peak and the reference peak and fitting them for shift parameters x_{act} and x_{ref} respectively. The movement of the actuated beam with respect to the substrate $\hat{x}_{\mathrm{act}}$ is then simply $\hat{x}_{\mathrm{act}} = x_{\mathrm{act}} - x_{\mathrm{ref}}$. Experimental results of non-differential measurements and an in-depth review of the influence of mechanical noise can be found elsewhere [25].

We have measured the position of two silicon beam springs of the nano-ram adhesion sensor. The motion of the left beam spring is equal to the motion of the ram, while the position of the right spring remains stationary with respect to the substrate. The voltage on the comb drive that moves the ram forward is increased from 0 V 60 V and back to 0 V in

2000 steps. The distance between consecutive voltage steps is decreased quadratically with increasing voltage to compensate for the characteristic quadratic voltage-displacement relation of the comb-drive actuator. The measured intensity profiles are summed over $N_{\text{lines}} = 367$ lines.

It is important to stress that the voltage is not swept in a continuous fashion, but in discrete steps. Each measurement point is obtained by sequentially setting the voltage, acquiring the image by exposing the sensor, and storing the intensity profile. The exposure time is 152 ms. Because the camera has a relatively slow data transfer rate, the time between set-acquire-store sequences is around 0.5 s.

In order to investigate what the position resolution of the curve-fitting technique is, we took a measurement of two stationary beams. Again, one is the 'moving' beam (even though in this case it is stationary) and the other is the reference beam. We measured the position of the moving beam with respect to the reference beam 200 times, for different values of N_{lines}. We executed this measurement using the 'Leiden MEMS tribometer' and the N-UNCD based adhesion sensor. The Leiden MEMS tribometer shows a better optical contrast than the nano-ram adhesion sensor that we used for the adhesion measurement. Compared to the silicon devices, the N-UNCD adhesion sensor's contrast is worse because the diamond device layer is slightly transparent.

9) Discrimination of Mechanical Noise: Because we do a differential position measurement using a stationary MEMS beam as an on-chip reference, low frequency mechanical vibrations of the sample with respect to the microscope will be rejected. The resonance frequencies of our MEMS structures (a few kilohertz) are orders of magnitude higher than the acquisition frame-rate (about 2 frames per second), so high frequency mechanical disturbances will 'average out' and translate to motion blur. To prevent this, the entire camera-microscope-sample assembly is suspended in bungee-cords inside an acoustic isolation booth on top of an active vibration isolated table. However, experiments carried out without any of these vibration isolation measures have shown that the influence of motion blur is not noticeable [25] and that our vibration isolation measures are not vital for a precise position measurement.

IV. Results and Discussion

A. Adhesion Measurement

The results of the adhesion sensor measurements are shown in figure 4. They show that the ram moves quadratically with the applied comb drive voltage until it touches the counter surface at 51.2 V. From lithography we know that the total gap between the ram and the counter surface is 2 µm. The ram displacement at the touching point is 26.9pixels, so the amount of nanometers per pixel is 74.4 nm/pixel.

When the voltage is decreased, it shows that at the point where the ram touched the counter surface during the forward motion, it now sticks to the counter surface until the voltage is decreased further down to 49.9 V, where the ram suddenly snaps-off, and displaces by 106.2 nm. We estimated the position noise of the measurement by fitting a 12$^{\text{th}}$ order

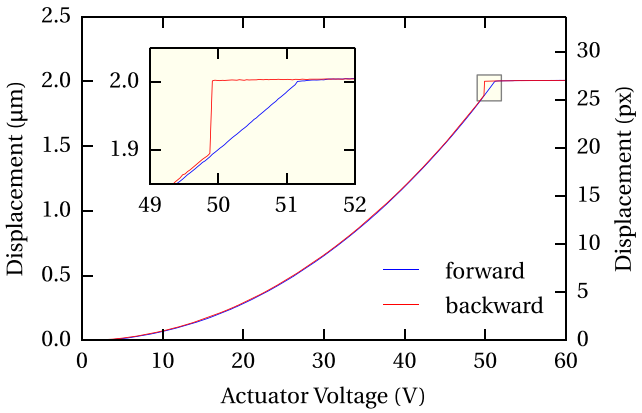

Fig. 4. Displacement of the ram towards the counter-surface and back to its initial position in the nano-ram adhesion sensor. At 51.2 V the ram touches the counter surface and stops moving. When the voltage is decreased, the ram adheres to the surface until it snaps off at 49.9 V and makes a jump of 106.2 nm ± 0.3 nm.

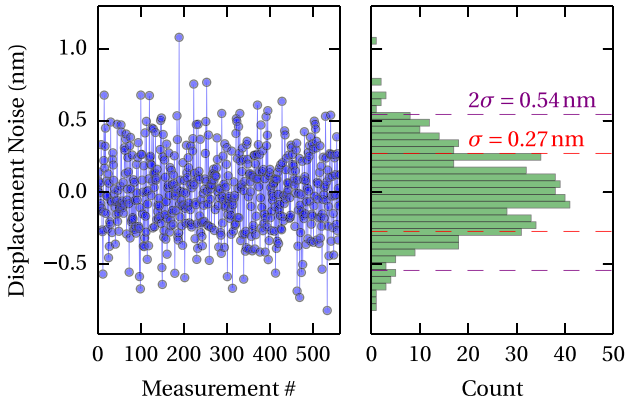

Fig. 5. The position noise of the nano-ram adhesion sensor measurement shown in Figure 4, calculated by subtracting a 12$^{\text{th}}$ order polynomial trend line from the parabolic part of the displacement curve. The standard deviation of the noise is $\sigma_{\text{pos}} = 0.27$ nm.

polynomial trend line through the displacement graph between 10 V to 45 V and subtracting it from the measurement. The high order of the polynomial was necessary to correct for thermal and charging effects (such as comb drive levitation) that cause the voltage-displacement relationship of the comb drive to deviate slightly from the ideal quadratic curve. The resulting position noise distribution is shown in figure 5. We calculated the standard deviation of the noise to be $\sigma_{\text{pos}} = 0.27$ nm.

B. Displacement Noise Measurements

Figure 6 shows the standard deviation of the position noise versus the number of averaged lines for the different devices. The standard deviation of the position noise of the silicon tribometer for a single line is 2.51nm and decreases with $\sqrt{\frac{1}{N_{\text{lines}}}}$ towards the lowest position noise we measured at $N_{\text{lines}} = 1577$, which is as low as 64 pm. The distribution of this measurement is shown in figure 7.

The standard deviation of the position noise of 0.27 nm that we calculated for the adhesion measurement (Figure 5) is shown as a single point in Figure 6 and is lies well above

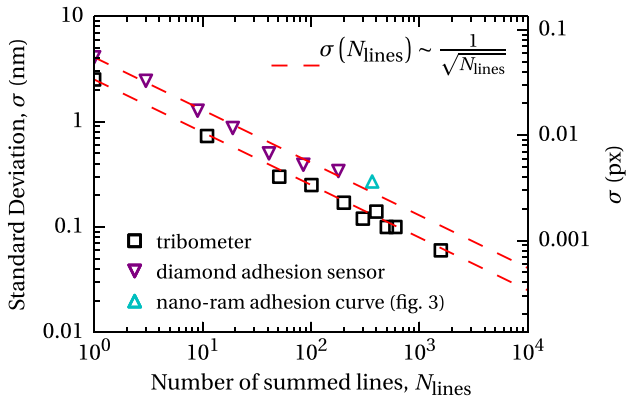

Fig. 6. Displacement error versus the number of summed lines (i.e. vertically binned pixels). The error decreases with a factor $\sqrt{\frac{1}{N_{\text{lines}}}}$.

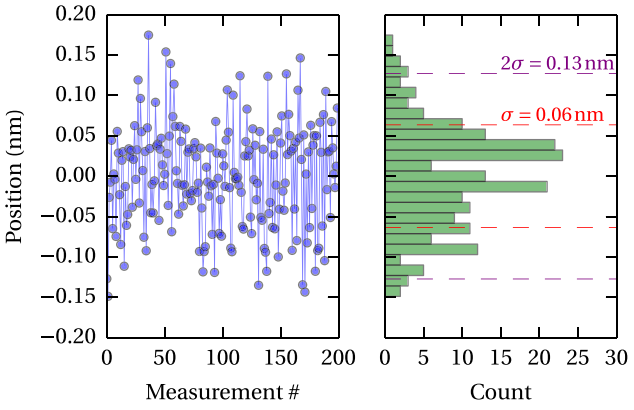

Fig. 7. Position noise measurement of the Leiden MEMS tribometer. The measured differential displacement of a stationary pair of silicon beams with $N_{\text{lines}} = 1577$ and a histogram that shows the distribution of the measured values in 25 bins. The standard deviation of the noise is $\sigma_{\text{pos}} = 64$ pm.

the trendline of the Leiden MEMS tribometer. The position uncertainty of the measurements taken with the N-UNCD adhesion sensors follows the same $\sqrt{\frac{1}{N_{\text{lines}}}}$ trend as the silicon tribometer, but has a larger error for the same amount of summed lines. Both these results are in accordance with the observation that the intensity profiles of the diamond device and the nano-ram adhesion sensor have a worse optical contrast than the silicon tribometer.

V. Conclusion

We have achieved an in-plane displacement resolution of 0.6 Å by fitting a shifted spline function through the intensity profile of a silicon beam that was imaged with an optical microscope and a CCD camera. The resolution depends strongly on the signal-to-noise ratio of the image. The noise figure is dominated by photon shot noise which is the limiting factor for the precision of the measurement. The effect of photon shot noise can be decreased by increasing the intensity of the light source, increasing the contrast, averaging or binning multiple lines, or by using a camera with a larger full-well-depth.

Compared to other optical in-plane displacement detection techniques, the curve fitting method presented in this paper offers the highest position resolution, although it was obtained using a large number of averaged image lines. It can be used to measure instantaneous 'jerky' motions of MEMS structures, something that is hard to accomplish with techniques that rely on spatio-temporal filtering. We have released our curve fitting procedure as an open source Python module [26] under the terms of the GNU General Public License. Images can be captured with any digital camera that fits onto a microscope, making this technique available to practically any laboratory.

Acknowledgments

The authors would like to thank Harry Jansen and Patrick van Holst for constructing the measurement setup.

References

[1] W. Kuehnel and S. Sherman, "A surface micromachined silicon accelerometer with on-chip detection circuitry," *Sens. Actuators A, Phys*, vol. 45, no. 1, pp. 7–16, Oct. 1994.

[2] E. M. Lawrence, K. E. Speller, and D. Yu, "MEMS characterization using laser doppler vibrometry," in *Proc. SPIE*, vol. 4980. 2003, pp. 51–62.

[3] S. Ellingsrud and G. O. Rosvold, "Analysis of a data-based TV-holography system used to measure small vibration amplitudes," *J. Opt. Soc. Amer. A*, vol. 9, no. 2, pp. 237–251, Feb. 1992.

[4] S. H. Wang, C. Quan, C. J. Tay, I. Reading, and Z. P. Fang, "Deformation measurement of MEMS components using optical interferometry," *Meas. Sci. Technol.*, vol. 14, no. 7, pp. 909–915, May 2003.

[5] M. R. Hart, R. A. Conant, Y. K. Lau, and R. S. Muller, "Stroboscopic interferometer system for dynamic MEMS characterization," *J. Microelectromech. Syst.*, vol. 9, no. 4, pp. 409–418, Dec. 2000.

[6] A. Bosseboeuf and S. Petitgrand, "Characterization of the static and dynamic behaviour of M(O)EMS by optical techniques: Status and trends," *J. Micromech. Microeng.*, vol. 13, no. 4, pp. S23–S33, Jun. 2003.

[7] G. F. LaVigne and S. L. Miller, "A performance analysis system for MEMS using automated imaging methods," in *Proc. IEEE Int. Test. Conf.*, Oct. 1998, pp. 442–447.

[8] B. Serio, J. J. Hunsinger, and B. Cretin, "In-plane measurements of microelectromechanical systems vibrations with nanometer resolution using the correlation of synchronous images," *Rev. Sci. Instrum.*, vol. 75, no. 10, pp. 3335–3341, Sep. 2004.

[9] A. Ya'akobovitz, S. Krylov, and Y. Hanein, "Nanoscale displacement measurement of electrostatically actuated micro-devices using optical microscopy and digital image correlation," *Sens. Actuators A, Phys.*, vol. 162, no. 1, pp. 1–7, Jul. 2010.

[10] C. Q. Davis and D. M. Freeman, "Using a light microscope to measure motions with nanometer accuracy," *Opt. Eng.*, vol. 37, no. 4, pp. 1299–1304, 1998.

[11] T. Guo, H. Chang, J. Chen, X. Fu, and X. Hu, "Micro-motion analyzer used for dynamic MEMS characterization," *Opt. Lasers Eng.*, vol. 47, nos. 3–4, pp. 512–517, Mar./Apr. 2009.

[12] A. Hafiane, S. Petitgrand, O. Gigan, S. Bouchafa, and A. Bosseboeuf, "Study of sub-pixel image processing algorithms for MEMS in-plane vibration measurements by stroboscopic microscopy," in *Proc. SPIE*, vol. 5145. 2003, pp. 169–179.

[13] S. Petitgrand and A. Bosseboeuf, "Simultaneous mapping of out-of-plane and in-plane vibrations of MEMS with (sub)nanometer resolution," *J. Micromech. Microeng.*, vol. 14, no. 9, pp. S97–S101, Aug. 2004.

[14] B. Kleinemeier, "Measurement of CCD interpolation functions in the subpixel precision range," in *Proc. SPIE*, vol. 1010. 1988, pp. 158–165.

[15] C. Q. Davis and D. M. Freeman, "Statistics of subpixel registration algorithms based on spatiotemporal gradients or block matching," *Opt. Eng.*, vol. 37, no. 4, pp. 1290–1298, Apr. 1998.

[16] C. Yamahata, E. Sarajlic, G. J. M. Krijnen, and M. A. M. Gijs, "Subnanometer translation of microelectromechanical systems measured by discrete fourier analysis of CCD images," *J. Microelectromech. Syst.*, vol. 19, no. 5, pp. 1273–1275, Oct. 2010.

[17] D. J. Burns and H. F. Helbig, "System for automatic electrical and optical characterization of microelectromechanical devices," *J. Microelectromech. Syst.*, vol. 8, no. 4, pp. 473–482, Dec. 1999.

[18] H. Yu, G. Zhou, S. K. Sinha, and F. S. Chau, "Scanning grating based in-plane movement sensing," *J. Micromech. Microeng.*, vol. 20, no. 8, p. 085007, Jul. 2010.
[19] A. Hachicha and S. Simon, "Subpixel edge detection for precise measurements by a vision system," in *Proc. SPIE*, vol. 1010, Feb. 1988, pp. 148–157.
[20] W. M. van Spengen and J. B. Roca, "On the noise limit of stress and temperature measurements with micro-raman spectroscopy," *J. Raman Spectrosc.*, vol. 44, no. 7, pp. 1039–1044, Jul. 2013.
[21] W. M. van Spengen and J. W. M. Frenken, "The leiden MEMS tribometer: Real time dynamic friction loop measurements with an on-chip tribometer," *Tribol. Lett.*, vol. 28, no. 2, pp. 149–156, 2007.
[22] W. M. van Spengen, "The accuracy of parameter estimation by curve fitting in the presence of noise," *J. Appl. Phys.*, vol. 111, no. 5, p. 054908, Mar. 2012.
[23] W. M. Van Spengen, G. H. C. J. Wijts, V. Turq, and J. W. M. Frenken, "Microscale friction reduction by normal force modulation in MEMS," *J. Adhes. Sci. Technol.*, vol. 24, nos. 15–16, pp. 2669–2680, 2010.
[24] F. Buja, A. V. Sumant, J. Kokorian, and W. M. van Spengen, "Electrically conducting ultrananocrystalline diamond for the development of a next generation of micro-actuators," *Sens. Actuators A, Phys.*, vol. 214, pp. 259–266, Aug. 2014.
[25] J. Kokorian, F. Buja, U. Staufer, and W. M. van Spengen, "An optical in-plane displacement measurement technique with sub-nanometer accuracy based on curve-fitting," in *Proc. IEEE 27th Int. Conf. Micro Electro Mech. Syst. (MEMS)*, Jan. 2014, pp. 580–583.
[26] J. Kokorian. (2014). *ODMAnalysis, a Python Package for the Analysis of Optical Displacement Measurements With Sub-Pixel Accuracy* [Online]. Available: https://github.com/jkokorian/ODMAnalysis/

Jaap Kokorian is currently pursuing the Ph.D. degree with the Delft University of Technology, Delft, The Netherlands. He received the Master's degree in electrical engineering from the University of Twente, Enschede, The Netherlands, in 2010. His current research is vapor-phase lubrication of MEMS devices, focusing on the study of atomic scale phenomena in friction, wear, and adhesion.

Federico Buja received the B.Sc. degree in aerospace engineering from the University of Padova, Padova, Italy, and the M.Sc. degree in nanotechnology and microsystems from the Heriot Watt University of Edinburgh, Edinburgh, U.K. He is currently a Ph.D. Researcher with the Delft University of Technology, Delft, The Netherlands. His main interest focuses on the investigation of micro and nano scale tribological phenomena in MEMS devices. The highlight of his research is the fabrication and study of ultrananocrystalline-based microactuators.

Willem Merlijn van Spengen received the degree in electrical engineering from the Eindhoven University of Technology, Eindhoven, The Netherlands, and the Ph.D. degree in applied science from Katholieke Universiteit Leuven, Leuven, Belgium, where he developed models for microscale adhesion and the effect of dielectric charging on MEMS switches. He continued his research at Leiden University, Leiden, The Netherlands, and is currently an Associate Professor with the Delft University of Technology, Delft, The Netherlands. His university research blends physics, chemistry, electronics, and micromechanics to understand the fundamental principles that govern microscale adhesion, friction, and wear. He is also the Director of Falco Systems BV, Amsterdam, The Netherlands, a company developing and producing high-voltage amplifiers for MEMS and piezo research.